A two-zone subgrid flame model for predicting the radiant emissions from fires

Soroush Rashidzadeh[a], Simo Hostikka[a], Randall McDermott[b,*]

[a]School of Engineering, Aalto University, Espoo, Finland

[b]National Institute of Standards and Technology, Gaithersburg, Maryland, USA

[*]Corresponding author: randall.mcdermott@nist.gov

Highlights:

- We introduce a simple subgrid model for temperature and absorption coefficient distribution which is consistent with the heat release rate from EDC.
- Model predictions for the radiative fraction of the UMD line burner experiments demonstrate improved accuracy and reduced grid dependency.
- Two-step fast chemistry model is used for predicting the in-flame soot concentrations.
- Model sensitivities to the assumed fuel carbon to CO fraction and the radiation model's path length are reported.

Abstract:

A simple two-zone subgrid temperature distribution is developed to model turbulence-radiation interaction in the Fire Dynamics Simulator. The new approach enforces consistency between the subgrid flame distribution and the heat release rate from the eddy dissipation model. To investigate the performance of the new model, we simulate the University of Maryland turbulent line burner and compare global radiative fraction as a function of coflow oxygen dilution. The results suggest that the model can improve grid resolution dependence in prediction of radiative emissions. Sensitivity of the model predictions to the assumed fuel carbon to CO fraction (a parameter of the two-step fast chemistry scheme) was found to be significant, which is not surprising since this parameter essentially controls the in-flame soot concentration and generally has a first-order effect on resolved emission. Four different model variations were tested, corresponding to varying degrees of complexity in modeling the subgrid correlations for the absorption coefficient. Differences in results between model implementations were on par with the variation in results obtained with different path lengths applied to the gray gas model for the absorption coefficient.

Keywords: Fire Dynamics Simulator; radiative fraction; turbulence-radiation interaction; subgrid temperature; soot

1. Introduction

A well-known problem in large-eddy simulation (LES) of fire engineering problems is that the flame temperatures cannot be adequately resolved and, consequently, the radiative emission cannot be accurately predicted. In practical fire calculations, this is usually handled by assigning a prescribed radiative fraction of the cell heat release to the source term of the radiative transfer equation (RTE). The influence of the subgrid-scale fluctuations in temperature and species composition on radiative emission and absorption is commonly known as turbulence radiation interaction (TRI).

TRI can be directly modeled (i.e., without prescribing a radiative fraction *a priori*) using Taylor expansion methods, transported (or direct) probability density function (PDF) methods (and the LES analog, filtered density function (FDF) methods [1]), or presumed-shape PDF/FDF methods. Gupta et al. [2] applied Taylor expansions to LES of a reacting channel flow and showed that absorption TRI can be neglected under certain conditions. Gupta et al. [3] used transported FDF to model turbulent jet flames. Chatterjee et al. [4] used a laminar smoke point method to determine in-flame soot concentrations and then applied Taylor expansion of the temperature field to close TRI. Xu et al. [5] used a presumed beta-FDF together with an unsteady flamelet library to close the chemical reaction and TRI terms in LES. Nmira et al. [6] showed the significance of subgrid TRI in non-luminous pool fires using a presumed beta-FDF method. Of the aforementioned studies, only one (Chaterjee et al. [4]) employed the eddy dissipation concept (EDC) combustion model, and none demonstrated filter-width independent (mesh independent) predictions of radiant emission.

The aim of this study is to propose and test a simple two-zone subgrid flame model that is consistent with the heat release rate from the EDC combustion model. It should improve the prediction of radiative quantities without employing computationally complex methods and achieve mesh independent solutions if large-scale features of the flow are reasonably well resolved. The model is implemented in the NIST Fire Dynamics Simulator (FDS) [7] and the University of Maryland (UMD) turbulent line burner [8] cases for methane and propane are simulated to validate the predictive capability and to assess the degree of mesh independence.

2. Model Formulation

2.1 Governing Equations

FDS solves the LES equations for mass, momentum, and energy in a low-Mach, variable density flow solver [7]. For the present paper, the equations of interest are the transport equations for Favre-filtered species mass fractions, $\tilde{Y}_\alpha$, and energy (sensible enthalpy), $\tilde{h}_s$,

$$\frac{\partial}{\partial t}(\overline{\rho}\,\tilde{Y}_\alpha) + \nabla\cdot(\overline{\rho}\,\tilde{Y}_\alpha\,\tilde{\mathbf{u}}) = -\nabla\cdot\mathbf{J}_{\alpha,sgs} - \nabla\cdot\tilde{\mathbf{J}}_\alpha + \overline{\dot{m}'''_\alpha} \tag{1}$$

$$\frac{\partial}{\partial t}(\overline{\rho}\,\tilde{h}_s) + \nabla\cdot(\overline{\rho}\,\tilde{h}_s\,\tilde{\mathbf{u}}) = \frac{\mathrm{D}\bar{p}}{\mathrm{D}t} + \overline{\dot{q}'''} - \nabla\cdot\dot{\mathbf{q}}''_{sgs} - \nabla\cdot\overline{\dot{\mathbf{q}}''} - \overline{\nabla\cdot\dot{\mathbf{q}}''_r} \tag{2}$$

Here, the filtered mass density is denoted $\overline{\rho}$; the Favre-filtered velocity is $\tilde{\mathbf{u}}$; $\overline{\mathbf{J}}_\alpha$ and $\mathbf{J}_{\alpha,sgs}$ are filtered molecular diffusive and subgrid-scale (unresolved) species mass fluxes, respectively. Similarly, in the energy equation $\overline{\dot{\mathbf{q}}''}$ and $\dot{\mathbf{q}}''_{sgs}$ are filtered heat flux and subgrid-scale heat flux vectors; $\bar{p}$ is the thermodynamic background pressure; and $\overline{\dot{q}'''}$ is the chemical heat release rate due to combustion, probably the most important term in fire dynamics. In these equations, both the mean chemical source term, $\overline{\dot{m}'''_\alpha}$ in (1), and the radiation source term, $-\overline{\nabla\cdot\dot{\mathbf{q}}''_r}$ in (2), are unclosed and must be modeled.

2.2 Closure of the Mean Chemical Source Term

2.2.1 Basic Eddy Dissipation Concept (EDC) Model for Turbulent Combustion

Consider a simple reaction between fuel (F) and air (A) to generate products (P),

$$\mathrm{F} + s\,\mathrm{A} \rightarrow (1+s)\,\mathrm{P} \tag{3}$$

Here, s is the mass stoichiometric ratio between the fuel and air. In the basic eddy dissipation model, we assume infinitely fast chemistry with the fuel and air initially unmixed (as in a diffusion flame). The rate of chemical reaction is then dictated by the rate of turbulent mixing, governed by the time scale, τ_{mix}. Details of the mixing time scale model are discussed in [7]. The rate of fuel consumption in the cell is given by [9, 10]

$$\overline{\dot{m}'''_{\mathrm{F}}} = -\overline{\rho}\,\frac{\min(\tilde{Y}_{\mathrm{F}}, \tilde{Y}_{\mathrm{A}}/s)}{\tau_{\mathrm{mix}}}, \tag{4}$$

and the heat release rate of the cell may be determined simply by multiplying by the fuel's heat of combustion (HOC):

$$\overline{\dot{q}'''} = -\overline{\dot{m}'''_{\mathrm{F}}} \times \mathrm{HOC} \tag{5}$$

2.2.2 Two-Step Fast Chemistry

McGrattan et al. [11] have proposed a two-step combustion model to predict CO and soot in under-ventilated fires. This two-step scheme is used throughout the work in this paper, as it affords an additional level of control over the in-flame soot concentration. The model postulates that CO and soot are produced in a fast initial step followed by oxidation to CO_2 in a slower second step. Since, Arrhenius rates are inaccurate in under-resolved flame calculations, the model exploits the idea that while the second oxidation step is slow relative to the first step, it is nevertheless still faster than the time step used in the combustion submodel. Thus, each reaction is treated as infinitely fast, but processed in serial, with the first reaction given priority for available oxygen.

As an example, consider propane combustion. Let γ denote the fraction of the fuel's carbon that is proportioned to CO versus soot[1] (here taken to be pure carbon, C). The two consecutive

[1] In an FDS input file, γ is set by the namelist parameter `FUEL_C_TO_CO_FRACTION`.

reaction steps are as follows:

$$C_3H_8 + (\tfrac{3}{2}\gamma + 2)\,O_2 \;\rightarrow\; 3\gamma CO + 3(1-\gamma)\,C + 4\,H_2O \tag{6}$$

$$3\gamma CO + 3(1-\gamma)\,C + 4\,H_2O + (3 - \tfrac{3}{2}\gamma)\,O_2 \;\rightarrow\; 3\,CO_2 + 4\,H_2O \tag{7}$$

Note that the default value of γ in FDS is $2/3$. The effect of this parameter on in-flame soot concentration and radiative emission is discussed later in this paper.

2.2.3 Ignition and Extinction

While the eddy dissipation model is robust, its shortcoming is that it generally requires *ad hoc* ignition and extinction criteria [12, 13]. The extinction model in FDS is based on the critical flame temperature (CFT) concept [14]. Details of the thermal extinction model are provided in [7]. A thorough discussion of ignition and extinction models is beyond the scope of this paper. However, it should be acknowledged that these issues may contribute to uncertainties in the radiation source term and cannot be wholly separated from TRI.

2.3 Closure of the Radiation Source Term

The radiation source term of the energy equation can be defined as the divergence of the spectral radiative heat flux integrated over the full spectrum

$$-\overline{\nabla \cdot \dot{\mathbf{q}}''_r} = \int_0^\infty \left(\overline{\kappa_\eta U_\eta} - \overline{4\pi\kappa_\eta I_{b\eta}}\right) \mathrm{d}\eta \tag{8}$$

where U_η is the local spectral incident intensity integrated over all directions, $U_\eta = \int_0^{4\pi} I_\eta \,\mathrm{d}\Omega$. After ignoring the spectral details (gray method [15]) and applying the spatial filter over the radiation source term, the emerging mathematical expression can be divided into two terms, $\overline{\kappa I}$ and $\overline{\kappa I_b}$, known as "absorption TRI" and "emission TRI," respectively. Due to nonlinear dependencies, these terms cannot be determined based on mean values of composition and temperature. However, in most cases the local intensity is weakly correlated with local absorption coefficient, and absorption TRI is here evaluated under the "optically thin fluctuation approxmiation" (OTFA): $\overline{\kappa U} \approx \overline{\kappa}\,\overline{U}$ [16].

Emission TRI can be decomposed into a resolved emission term and three subgrid correlations:

$$\underbrace{\overline{\kappa(\mathbf{Y},T)I_b(T)}}_{\text{Emission TRI}} = \underbrace{\kappa(\widetilde{\mathbf{Y}},\widetilde{T})I_b(\widetilde{T})}_{\text{Resolved Emission}} + \underbrace{[\overline{\kappa(\mathbf{Y},T)} - \kappa(\widetilde{\mathbf{Y}},\widetilde{T})]I_b(\widetilde{T})}_{\mathscr{C}_\kappa}$$

$$+ \underbrace{\overline{\kappa(\mathbf{Y},T)}[\overline{I_b(T)} - I_b(\widetilde{T})]}_{\mathscr{C}_T} + \underbrace{[\overline{\kappa(\mathbf{Y},T)I_b(T)} - \overline{\kappa(\mathbf{Y},T)}\,\overline{I_b(T)}]}_{\mathscr{C}_{\kappa-T}} \tag{9}$$

where $\widetilde{\mathbf{Y}}$ and $\widetilde{T}$ are Favre-filtered composition and temperature, respectively. Each $\mathscr{C}$ term corresponds to a different type of subgrid correlation: $\mathscr{C}_\kappa$ and $\mathscr{C}_T$ represent the self correlations of

absorption coefficient and temperature, respectively, and $\mathscr{C}_{\kappa-T}$ contains the cross-correlation between absorption coefficient and temperature.

2.3.1 Two-Zone Subgrid Temperature Model

The computational cell is decomposed into two zones: a flame zone at flame temperature T_f and an unburned reactant zone at temperature T_u, taken as the initial cell temperature at the start of the combustion substep (see Fig. 1). An algorithm to compute the flame temperature is provided in Appendix A; for our purposes here, assume T_f is known.

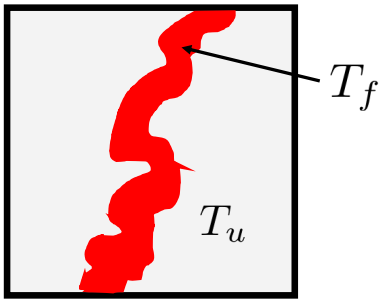

Fig. 1. Two-zone decomposition of a computational cell.

To be consistent with the spatial filter applied to the LES equations, the subgrid distribution is weighted by volume fraction of the flame and unburned zones. The implied marginal filtered density function [1] for temperature may be written as,

$$f(\theta) = X_u \delta(T_u - \theta) + X_f \delta(T_f - \theta) \quad ; \quad X_u + X_f = 1 \tag{10}$$

where X_u and X_f are the unburned and flame zone volume fractions.

2.3.2 EDC Consistent Flame Zone Model

The key contribution of this paper is to enforce consistency between the subgrid temperature distribution and the heat release rate from the EDC model. This is done simply by computing a flame zone mass fraction, here denoted Z_f, from the flame temperature and the heat release rate,

$$Z_f = \frac{\dot{q}''' \Delta t}{\overline{\rho}(c_{p,f} T_f - c_{p,u} T_u)} \tag{11}$$

The flame volume fraction is then computed as

$$X_f = Z_f \frac{\overline{W}_u}{\overline{W}_f} \frac{T_f}{T_u} \tag{12}$$

where $\overline{W}_u$ is the mean molecular weight of the cell prior to integration of the combustion model (i.e., the initial state of the cell) and $\overline{W}_f$ is the mean molecular weight of the flame zone. The composition of the flame zone, $\mathbf{Y}_f$, is discussed in Appendix A.

2.3.3 TRI Implementation

Based on the subgrid decomposition of the emission TRI term outlined in Eq. (9), we consider four different modeling approaches, corresponding to varying degrees of complexity in the subgrid distribution:

TRI-0: In the first approach, only $\mathscr{C}_T$ is taken into account and other correlations are neglected. Absorption coefficient is evaluated at initial cell species concentration and temperature.

$$\begin{aligned}\overline{\kappa(\mathbf{Y},T)I_b(T)} &\approx \kappa(\widetilde{\mathbf{Y}},\widetilde{T})I_b(\widetilde{T}) + \overline{\kappa(\mathbf{Y},T)}[\overline{I_b(T)} - I_b(\widetilde{T})] \\ &\approx \frac{\sigma}{\pi}\kappa(\widetilde{\mathbf{Y}_u},\widetilde{T_u})(X_u\,\widetilde{T_u}^4 + X_f\,\widetilde{T_f}^4)\end{aligned} \tag{13}$$

TRI-1: This approach is similar to TRI-0 except that the absorption coefficient is evaluated at the mean species composition and temperature of the cell.

$$\begin{aligned}\overline{\kappa(\mathbf{Y},T)I_b(T)} &\approx \kappa(\widetilde{\mathbf{Y}},\widetilde{T})I_b(\widetilde{T}) + \overline{\kappa(\mathbf{Y},T)}[\overline{I_b(T)} - I_b(\widetilde{T})] \\ &\approx \frac{\sigma}{\pi}\kappa(\widetilde{\mathbf{Y}},\widetilde{T})(X_u\,\widetilde{T_u}^4 + X_f\,\widetilde{T_f}^4)\end{aligned} \tag{14}$$

TRI-2: Absorption coefficient can be evaluated at different conditions for each zones of the temperature model. Consequently, $\mathscr{C}_T$ and $\mathscr{C}_{\kappa-T}$ are modeled.

$$\begin{aligned}\overline{\kappa(\mathbf{Y},T)I_b(T)} &\approx \kappa(\widetilde{\mathbf{Y}},\widetilde{T})I_b(\widetilde{T}) + \overline{\kappa(\mathbf{Y},T)}[\overline{I_b(T)} - I_b(\widetilde{T})] + [\overline{\kappa(\mathbf{Y},T)I_b(T)} - \overline{\kappa(\mathbf{Y},T)}\,\overline{I_b(T)}] \\ &\approx \frac{\sigma}{\pi}(X_u\,\kappa(\widetilde{\mathbf{Y}},\widetilde{T_u})\,\widetilde{T_u}^4 + X_f\,\kappa(\widetilde{\mathbf{Y}},\widetilde{T_f})\,\widetilde{T_f}^4)\end{aligned} \tag{15}$$

TRI-3: The most inclusive version of TRI can be obtained by assuming that absorption coefficient can be evaluated at different species composition and temperature for each zone. With this approach all three correlations of $\mathscr{C}_T$, $\mathscr{C}_\kappa$ and $\mathscr{C}_{\kappa-T}$ are accounted for and modelled.

$$\overline{\kappa(\mathbf{Y},T)I_b(T)} \approx \frac{\sigma}{\pi}(X_u\,\kappa(\widetilde{\mathbf{Y}}_u,\widetilde{T_u})\,\widetilde{T_u}^4 + X_f\,\kappa(\widetilde{\mathbf{Y}}_f,\widetilde{T_f})\,\widetilde{T_f}^4) \tag{16}$$

3. Validation Target: The University of Maryland Turbulent Line Burner

In order to investigate the performance of the two-zone model, a series of simulations are conducted on the turbulent line burner of developed at the University of Maryland (UMD) [8]. The UMD line burner, 50 cm long by 5 cm wide with a 2.5 cm ceramic flame holder, is a 50 kW turbulent diffusion flame, fueled by methane or propane, with controlled inlet and boundary conditions. Varying combustion efficiency and radiative fraction, and finally suppression of the line burner, are achieved by adding nitrogen to the oxidizer stream. Visible flame height, oxygen mole fraction and infrared emission are measured quantities of the experiment [17] (see Fig. 2(a) for an image of the flame).

The FDS simulations are performed with three different grid resolutions dividing the fuel port width, $W = 5$ cm, into 4, 8 and 16 cells, respectively. The chemical reaction is based on the two-step fast chemistry model. Post flame yields for CO and soot were set to zero for methane. For propane, the SFPE handbook [18] values of $y_{CO} = 0.005$ and $y_{soot} = 0.024$ are used. We use 400 solid angles in the RTE with 1/20th of the intensities updated once every three time steps (this angular resolution is chosen based on a previous convergence study in [12]; a full RTE update is obtained every 60 time steps; for the medium resolution case, with $\Delta t \approx 5 \times 10^{-4}$ s, this results in a full radiation update every 0.03 s).

For extinction, the critical flame temperatures for methane and propane are set to SFPE handbook [18] values of 1507 °C and 1447 °C, respectively. The ignition zone is set to 5 cm above the burner using the method described in [12]. The ignition threshold temperature is set to 450 °C for both methane and propane. The burner surface temperature (also the fuel inlet temperature) is set to 600 °C based on extrapolation of in-flame temperatures measured by McCaffrey [19, 20]. The ignition volume, ignition threshold temperature, and burner surface temperatures all contribute to the combustion efficiency near the oxygen depletion cutoff. The values selected here allowed for coarse mesh cases to maintain combustion up to the cutoff for both methane and propane fuels. Results for combustion efficiency are presented in Sec. 4.1 below.

In the experiments, the radiative fractions were determined using heat flux gauges and a weighted multi-point radiation source model. The simulated radiative fractions, in turn, were calculated by integrating the radiative source term, Eq. (8), over the domain volume and dividing by the burner fuel flow rate times the heat of combustion (note: this matches the method used to report χ_R in [8]),

$$\chi_R = \frac{\int -\overline{\nabla \cdot \dot{\mathbf{q}}_r''}\, dV}{\dot{m}_F \times \mathrm{HOC}} \tag{17}$$

4. Results and Discussion

4.1 Flame Structure and Combustion Efficiency

Before focusing on the performance of the TRI model implementations, we must ensure that the model without any TRI implementation reproduces the key general characteristics of the UMD line burner experiments. Figure 2 depicts an instantaneous flame structure in simulation and experiment at the same O_2 volume fraction. Similarity between the flame height and its structure is evident. Mean thermocouple temperatures across the width of the methane flame at two vertical positions are illustrated in Fig. 3 for different grid resolutions, showing the agreement between experimental data and numerical simulation. The combustion efficiency represented in Fig. 4 shows uncertainty in predicting the final stage of the suppression process and grid dependency in the predicted O_2 concentration at which the combustion stops. It should be acknowledged that the ignition volume and threshold temperature are not well defined properties of the simulation, and that ignition models are still a subject of active research in the fire science community.

(a) (b)

Fig. 2. UMD Line Burner methane flame structure at 18 vol.% O_2 in co-flow. (a) Experiment [8] (reproduced with permission from the author), (b) Fine resolution simulation showing volume rendering of heat release rate per unit volume (above 200 kW/m^3).

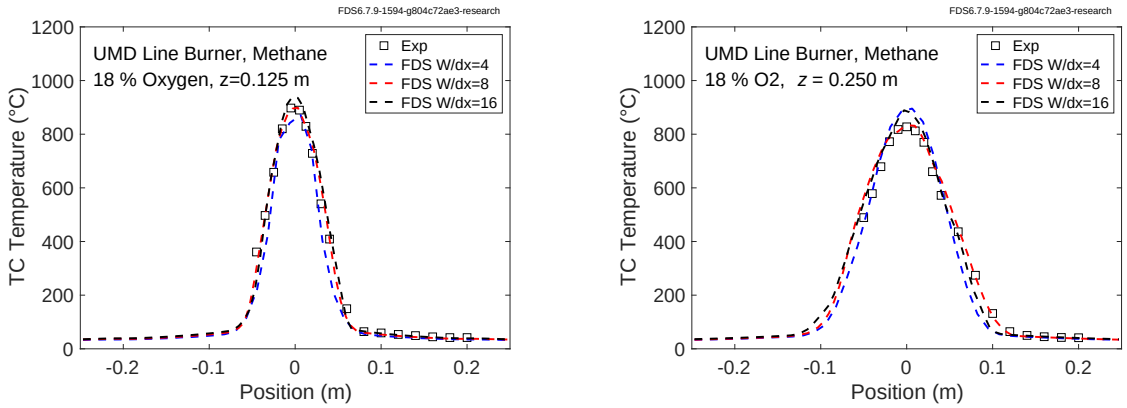

(a) (b)

Fig. 3. Mean thermocouple temperature profiles (a) at 12.5 cm and (b) 25.0 cm above the burner in methane flame (no TRI model).

4.2 Comparison between TRI implementations

To test the variability in TRI implementation, we compared predictions of radiative fraction at coarse grid resolution for TRI-0 through TRI-3. The results are shown in Fig. 5 for methane and propane flames. They suggest that at higher oxygen volume fractions, TRI-0 and TRI-1 predict higher radiative fraction compared to TRI-2 and TRI-3. This means allowing for other correlations will yield lower χ_R, which is consistent with claims made in [21, 22] arguing that for most diffusion flames, turbulent subgrid-scale effects reduce the absorption coefficient and the net effect on $\mathscr{C}_\kappa$ is to reduce its value.

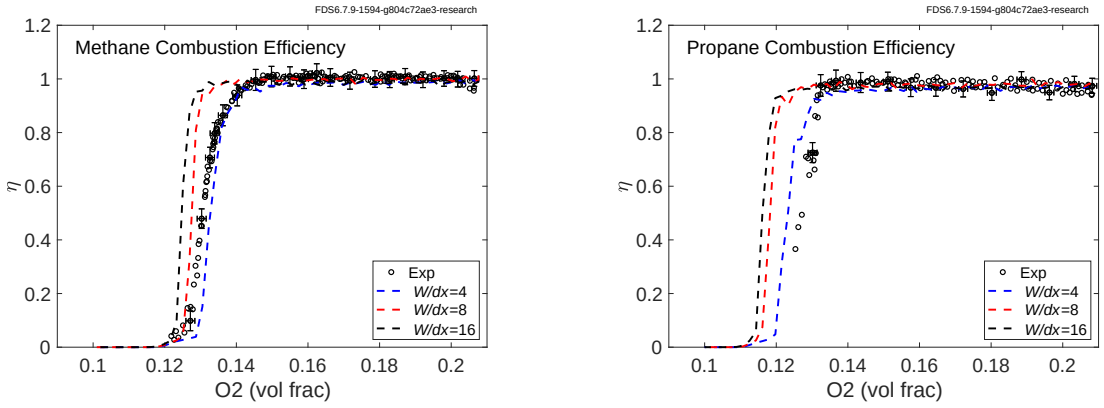

(a) (b)

Fig. 4. Combustion efficiency (no TRI model) for (a) methane and (b) propane.

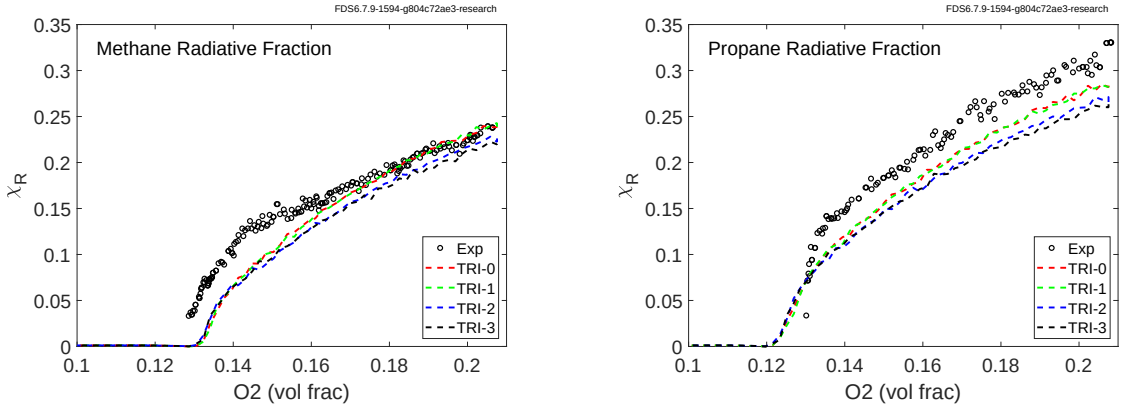

(a) (b)

Fig. 5. Radiative fraction with different TRI versions, (a) methane, (b) propane, at coarse grid resolution ($\Delta x = 1.25$ cm, $W/\Delta x = 4$).

4.3 Grid dependence analysis with TRI-0 and TRI-3

The performance of TRI-0 and TRI-3 with different grid resolutions is investigated in Fig. 6. In the baseline simulations, although the radiative fraction trend is captured with all grid resolutions, the quantitative values are significantly dependent on the grid size. TRI-0 results are clearly less grid dependent. The effect of TRI-0 on the radiative fraction predictions is pronounced for the coarsest mesh and diminishes as the grid is refined. In the case of TRI-3, improvements over baseline are much more subtle. A possible explanation behind this discrepancy is the fact that the absorption coefficient defined for the flame region in TRI-3 (Eq. 16) must be evaluated with its corresponding path length. The role of the path length and its significance in obtaining radiative properties is addressed in Sec. 4.4. Other possible explanations for the mesh sensitivity of TRI-3, (for example, the constraints implied by a complete joint filtered density function of composition and temperature) are being investigated, but are beyond the scope of the present paper.

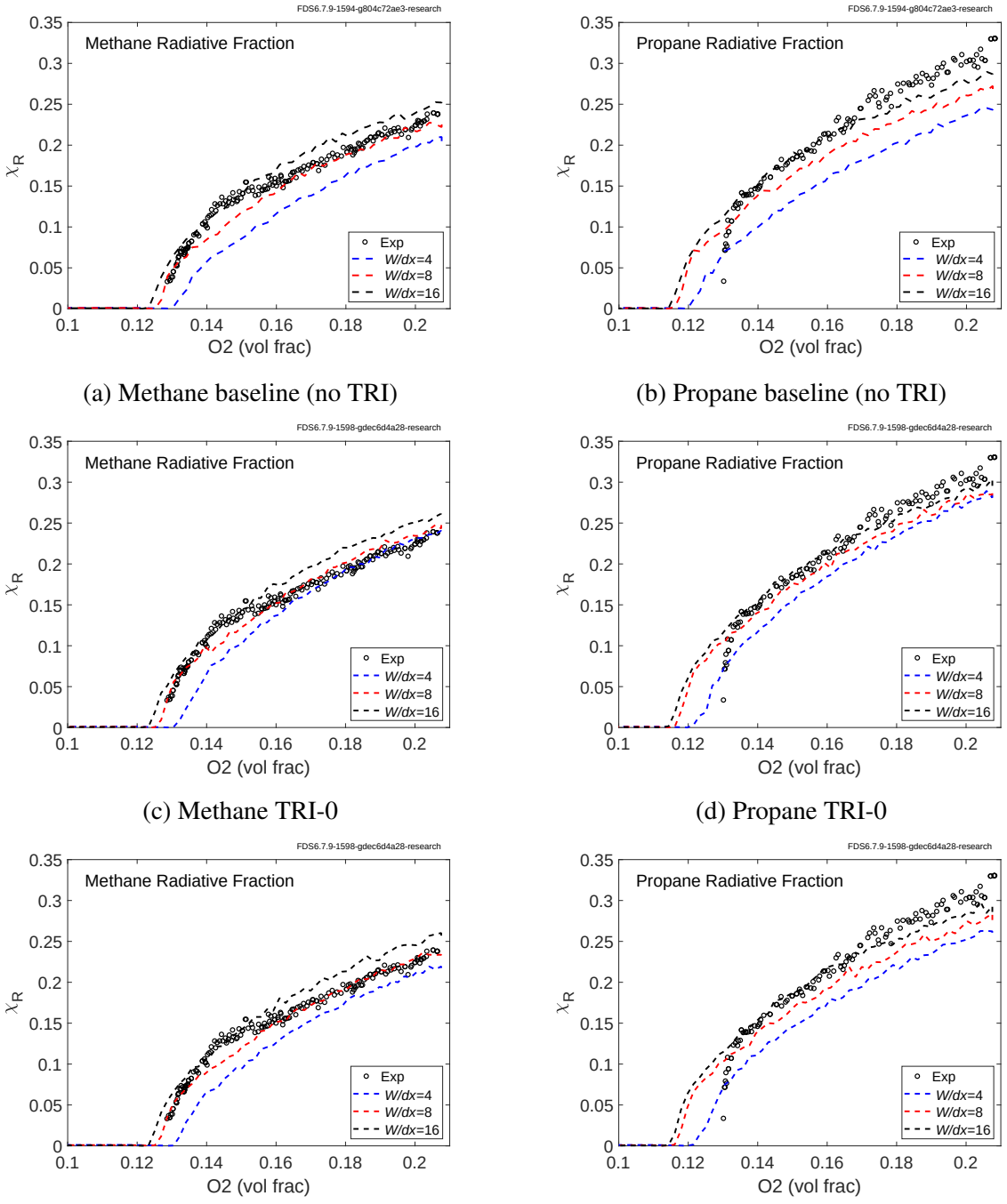

(a) Methane baseline (no TRI)

(b) Propane baseline (no TRI)

(c) Methane TRI-0

(d) Propane TRI-0

(e) Methane TRI-3

(f) Propane TRI-3

Fig. 6. Radiative fraction for different fuels and grid resolutions, (a) and (b) Baseline, (c) and (d) TRI-0, (e) and (f) TRI-3.

The local influence of the TRI model may be measured through a TRI correction factor defined as the ratio of full TRI to emission TRI,

$$\mathscr{R}_{TRI} = \overline{\kappa(\mathbf{Y},T)I_b(T)}/\kappa(\widetilde{\mathbf{Y}},\widetilde{T})I_b(\widetilde{T}) \tag{18}$$

Figure 7 shows instantaneous slices of the TRI correction at 18 vol. % O_2 for TRI-0 used to model the UMD line burner propane flame. These images provide qualitative support for the model behavior, as we can see high levels of TRI occuring near the flame envelop where we expect high soot concentration on the rich side of the flame intersecting with high temperature values. It is evident from the comparison of different grid resolutions that the ratio of computational cells affected by higher values of $\mathscr{R}_{TRI}$ increases for coarse grid resolution. The colorbar limits are set for visualization purposes; however, within the code $\mathscr{R}_{TRI}$ is allowed to vary between 0 and 100. Generally, min and max values experienced by the solver are on the order of 0.5 and 10, respectively[2].

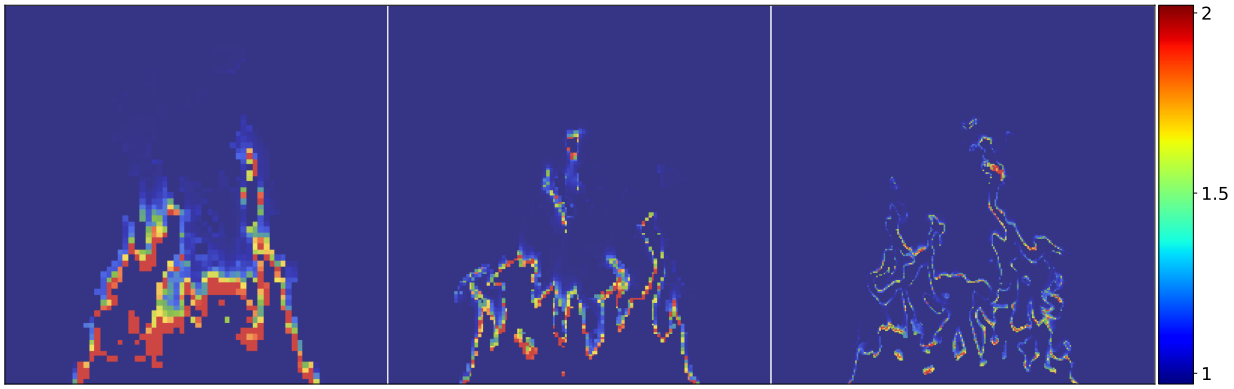

Fig. 7. Instantaneous slice of TRI correction factor $\mathscr{R}_{TRI}$ (see Eq. (18)) for propane at 18 vol. % O_2, coarse (left), medium (middle), and fine (right) grid resolutions.

4.4 Effects of the first reaction CO/soot ratio and path length

The parameter γ, the fraction of the fuel's carbon apportioned to CO versus soot (see reaction Eqs. (6) and (7)), plays an influential role in determining the in-flame soot concentration in the two-step combustion model. The sensitivity of the predicted radiative fraction on this parameter is studied by carrying out a series of coarse mesh propane simulations with TRI-3 and four different values of γ between 0 and 1. The results are shown in Fig. 8(a). A value of $\gamma = 0$ means all the carbon in the first step becomes soot in the first reaction, which leads to the highest χ_R due to the strong emissivity of soot. In case of $\gamma = 1$, where no soot is produced in the first combustion step, the radiative emissions are severely underestimated. As discussed in McGratten et al. [11], there is as of yet no strong theoretical or direct empirical justification for a particular value; to some extent, γ can be seen as a calibration coefficient. Due to the strong coupling between the radiative and other thermodynamic quantities, all the possible data should be examined in light of the calibration, which is beyond the scope of the present publication.

FDS uses the RadCal [23, 7] narrow band-model to obtain the effective gray absorption coefficients for the gas species and soot over a range of possible concentrations and temperatures. When computing an effective absorption coefficient, RadCal requires a path length which has a default

[2] Values of $\mathscr{R}_{TRI} < 1$ are possible when flame κ values are smaller than resolved values.

value of 10 cm in FDS. A sensitivity study showing the role of path length is shown in Fig. 8(b). For the TRI-3 implementation at coarse grid resolution, the study demonstrates that the effect of the chosen path length on radiative fraction, between 2 cm and 20 cm, of the same order importance as the TRI implementation, which leads to the conclusion that, in order to improve radiation predictions, it may be necessary to move towards non-gray global radiation models that eliminate the role of the path length.

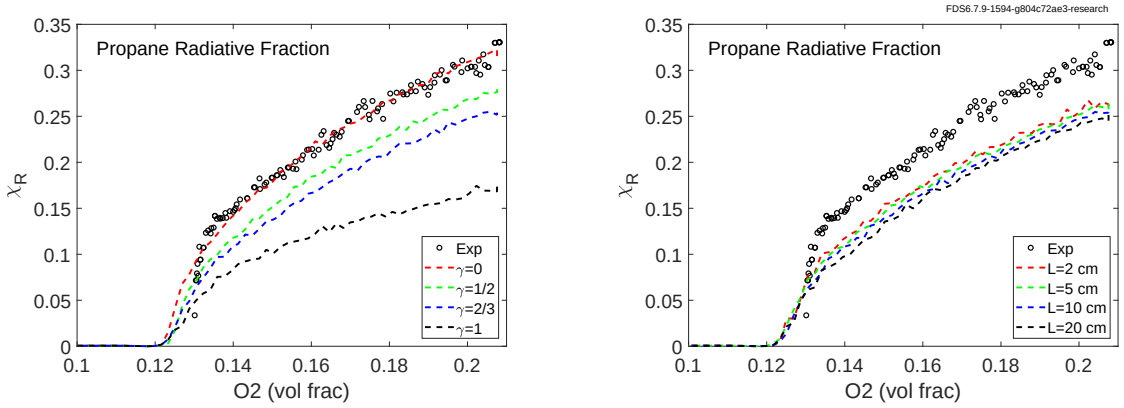

(a) (b)

Fig. 8. Effect of (a) the fuel carbon to CO fraction γ, and (b) path length on the Propane flame radiative fraction at coarse grid resolution ($\Delta x = 1.25$ cm, $W/\Delta x = 4$) using TRI-3.

5. Conclusions

This study presents a simple two-zone subgrid model for flame properties to address turbulence radiation interaction in fire simulations. The mdoel is constructed to enforce consistency between the flame temperature, the flame volume fraction, and the heat release rate from the EDC combustion model. Four alternative approaches for evaluating the gray absorption coefficients inside and outside the subgrid flame zone are implemented in FDS. The UMD line burner is chosen as the validation target. Baseline calculations show reasonably good agreement with in-flame mean temperatures at three grid resolutions. Flame structure and combustion efficiency are checked for good baseline model performance.

Overall, the results suggest that the TRI models presented in this work provide better radiative fraction predictions than the baseline model at all grid resolutions. Using the TRI model reduces grid dependency, especially at higher oxygen concentrations, but uncertainties in the combustion efficiency at the extinction limit hamper the assessment of radiation quantities. These problems are related to the modeling of ignition and extinction processes.

Superior performance of TRI-0 compared to the theoretically more complete TRI-3 can, at least partially, be explained by the role of path length in obtaining radiative properties. Connecting the zone properties to state and boundary conditions of the underlying RadCal model includes

open questions that could not be explored in the current study. Both the theoretical difficulties and observed path length sensitivity in the predictions indicate the need to move towards non-gray global modeling of radiative properties.

Based on these reasonable validation results, the previously developed two-step combustion model seems to yield realistic in-flame concentrations for the radiating species. However, the sensitivity of the radiative fractions to the assumed fuel carbon to CO fraction, γ, indicates the need for further research to optimize and justify value for different fuels and conditions.

A. Flame Temperature Model

Computation of the adiabatic flame temperature is straight forward, given an initial and final composition and an initial temperature. The "modeling" aspect involves determination of the diffusion flame composition, which is different from the initial cell composition (a homogeneous cell composition would imply a premixed flame). We interpret the flame zone as a "stoichiometric pocket" of reactants. This composition may differ from a stoichiometric fuel-air mixture due to possible dilution from combustion products or other agents.

Let $[Y_F^0, Y_A^0, Y_P^0]$ and $[Y_F, Y_A, Y_P]$ denote the cell mass fractions of fuel, air, and products, respectively, before and after the integration of the combustion model. The local equivalence ratio in the stoichiometric pocket of the reactor is

$$\tilde{\phi} \equiv \frac{s Y_F^0}{Y_A^0} = \begin{cases} \dfrac{Y_A^0 - Y_A}{Y_A^0} & \text{if} \quad Y_A > 0 \quad \text{(excess air)} \\ \\ \dfrac{Y_F^0}{Y_F^0 - Y_F} & \text{if} \quad Y_F > 0 \quad \text{(excess fuel)} \end{cases} \tag{19}$$

where s is the mass stoichiometric coefficient of air. This definition of the equivalence ratio omits both excess fuel and excess air from the stoichiometric pocket (flame zone).

A.1 Excess Air

In the case of excess air ($\tilde{\phi} < 1$), the flame zone reaction equation may be written as

$$Y_F^0 + \tilde{\phi}(Y_A^0 + Y_P^0) \rightarrow Y_P - (1 - \tilde{\phi})\, Y_P^0 \tag{20}$$

Conservation of total enthalpy in the flame zone is then governed by,

$$Y_F^0\, h_F(T_u) + \tilde{\phi}(Y_A^0\, h_A[T_u] + Y_P^0\, h_P[T_u]) = [Y_P - (1 - \tilde{\phi}) Y_P^0]\, h_P(T_f) \tag{21}$$

Here, T_f is the adiabatic flame temperature. Given functions for enthalpy, which include the enthalpy of formation, Eq. 21, is solved with a nonlinear solution procedure (a Newton method) to determine T_f.

On a 1 kg basis for the cell, a total mass of $(1-\tilde{\phi})(Y_A^0+Y_P^0)$ has been omitted from the flame zone. The resulting "flame composition" is obtained by renormalizing the product composition (which may contain multiple tracked species), let $\hat{\mathbf{Y}}_P = \mathbf{Y}_P - (1-\tilde{\phi})\mathbf{Y}_P^0$, then $\mathbf{Y}_f = \hat{\mathbf{Y}}_P / \sum(\hat{\mathbf{Y}}_P)$.

A.2 Excess Fuel

In the case of excess fuel ($\tilde{\phi} > 1$), the flame zone reaction equation may be written as

$$(1/\tilde{\phi})(Y_F^0+Y_P^0)+Y_A^0 \rightarrow Y_P-(1-1/\tilde{\phi})Y_P^0 \tag{22}$$

The energy equation for the flame zone becomes,

$$(1/\tilde{\phi})(Y_F^0 h_F(T_u)+Y_P^0 h_P[T_u])+Y_A^0 h_A[T_u] = [Y_P-(1-1/\tilde{\phi})Y_P^0]\,h_P(T_f) \tag{23}$$

On a 1 kg basis, $(1-1/\tilde{\phi})(Y_F^0+Y_P^0)$ has been omitted from the flame zone. The resulting flame composition, with $\hat{\mathbf{Y}}_P = \mathbf{Y}_P - (1-1/\tilde{\phi})\mathbf{Y}_P^0$, is $\mathbf{Y}_f = \hat{\mathbf{Y}}_P / \sum(\hat{\mathbf{Y}}_P)$.

Acknowledgements

This work was funded in part by the Scientific and Technical Research and Services (STRS) Laboratories Program, Advanced Fire Modeling project at NIST. At Aalto University, this work was supported by the Finnish Fire Protection Fund (Palosuojelurahasto) and CSC - IT Center for Science Ltd. The authors would like to thank James White for permission to use the flame images of the UMD line burner.

References

[1] P.J. Colucci, F.A. Jaberi, P. Givi, and S.B. Pope. Filtered density function for large eddy simulation of turbulent reacting flows. *Phys. Fluids*, 10(2):499–515, 1998. 2, 5

[2] A. Gupta, M.F. Modest, and D.C. Haworth. Large-eddy simulations of turbulence-radiation interactions in a turbulent planar channel flow. *Journal of Heat Transfer*, 131(1):061704–1–8, 2009. 2

[3] A Gupta, DC Haworth, and MF Modest. Turbulence-radiation interactions in large-eddy simulations of luminous and nonluminous nonpremixed flames. *Proceedings of the Combustion Institute*, 34(1):1281–1288, 2013. 2

[4] Prateep Chatterjee, Yi Wang, Karl V Meredith, and Sergey B Dorofeev. Application of a subgrid soot-radiation model in the numerical simulation of a heptane pool fire. *Proceedings of the Combustion Institute*, 35(3):2573–2580, 2015. 2

[5] Rui Xu, Alexis Marchand, Salman Verma, Thomas Rogaume, Franck Richard, Jocelyn Luche, Arnaud Trouvé, et al. Simulations of the coupling between combustion and radiation in a turbulent line fire using an unsteady flamelet model. *Fire Safety Journal*, 120:103101, 2021. 2

[6] Fatiha Nmira, Li Ma, and Jean-Louis Consalvi. Assessment of subfilter-scale turbulence-radiation interaction in non-luminous pool fires. *Proceedings of the Combustion Institute*, 38(3):4927–4934, 2021. 2

[7] K. McGrattan, S. Hostikka, R. McDermott, J. Floyd, C. Weinschenk, and K. Overholt. *Fire Dynamics Simulator, Technical Reference Guide, Volume 1: Mathematical Model*. National Institute of Standards and Technology, Gaithersburg, Maryland, USA, and VTT Technical Research Centre of Finland, Espoo, Finland, sixth edition, September 2013. 2, 3, 4, 11

[8] James P. White. *Measurement and Simulation of Suppression Effects in a Buoyant Turbulent Line Fire*. PhD thesis, University of Maryland, College Park, Maryland, 2016. 2, 6, 7, 8

[9] B.F. Magnussen and B.H. Hjertager. On Mathematical Modeling of Turbulent Combustion with Special Emphasis on Soot Formation and Combustion. In *Proceedings of the Sixteenth Symposium (International) on Combustion*, pages 719–729. Combustion Institute, Pittsburgh, Pennsylvania, 1977. 3

[10] T. Poinsot and D. Veynante. *Theoretical and Numerical Combustion*. R.T. Edwards, Inc., Philadelphia, Pennsylvania, 2nd edition, 2005. 3

[11] K. McGrattan, R. McDermott, and J. Floyd. A Simple Two-Step Reaction Scheme for Predicting CO in Under-Ventilated Compartments. In *Proceedings of the Tenth International Symposium on Fire and Explosion Hazards*, Oslo, Norway, 2022. 3, 11

[12] J. P. White, S. Vilfayeau, A. W. Marshall, A. C. Trouvé, and R. J. McDermott. Modeling flame extinction and reignition in large eddy simulations with fast chemistry. *Fire Safety Journal*, 90:72–85, 2017. 4, 7

[13] S. Vilfayeau, J.P. White, P.B. Sutherland, A.W. Marshall, and A. Trouvé. Large eddy simulation of flame extinction in a turbulent line fire exposed to air-nitrogen co-flow. *Fire Safety Journal*, 86:16–31, 2016. 4

[14] C. Beyler. *SFPE Handbook of Fire Protection Engineering*, chapter Flammability Limits of Premixed and Diffusion Flames. Springer, New York, 5th edition, 2016. 4

[15] Fengshan Liu, Jean-Louis Consalvi, and Fatiha Nmira. The importance of accurately modelling soot and radiation coupling in laminar and laboratory-scale turbulent diffusion flames. *Combustion and Flame*, page 112573, 2022. 4

[16] Pedro J Coelho. Numerical simulation of the interaction between turbulence and radiation in reactive flows. *Progress in energy and combustion science*, 33(4):311–383, 2007. 4

[17] JP White, ED Link, AC Trouvé, PB Sunderland, AW Marshall, JA Sheffel, ML Corn, MB Colket, M Chaos, and H-Z Yu. Radiative emissions measurements from a buoyant, turbulent line flame under oxidizer-dilution quenching conditions. *Fire Safety Journal*, 76:74–84, 2015. 6

[18] M.J. Hurley, editor. *SFPE Handbook of Fire Protection Engineering*. Springer, New York, 5th edition, 2016. 7

[19] B.J. McCaffrey. Purely Buoyant Diffusion Flames: Some Experimental Results. NBSIR 79-1910, National Bureau of Standards (now NIST), Gaithersburg, Maryland, October 1979. 7

[20] K. McGrattan, S. Hostikka, R. McDermott, J. Floyd, C. Weinschenk, and K. Overholt. *Fire Dynamics Simulator, Technical Reference Guide, Volume 3: Validation*. National Institute of Standards and Technology, Gaithersburg, Maryland, USA, and VTT Technical Research Centre of Finland, Espoo, Finland, sixth edition, September 2013. 7

[21] Michael F Modest and Daniel C Haworth. *Radiative heat transfer in turbulent combustion systems: theory and applications*. Springer, 2016. 8

[22] Jean-Louis Consalvi, Fatiha Nmira, and Wenjun Kong. On the modeling of the filtered radiative transfer equation in large eddy simulations of lab-scale sooting turbulent diffusion flames. *Journal of Quantitative Spectroscopy and Radiative Transfer*, 221:51–60, 2018. 8

[23] W. Grosshandler. RadCal: A Narrow Band Model for Radiation Calculations in a Combustion Environment. NIST Technical Note 1402, National Institute of Standards and Technology, Gaithersburg, Maryland, 1993. 11